Three dimensional nanoporous density graded materials formed by optical exposures through conformable phase masks

Seokwoo Jeon, Yun-Suk Nam, Daniel Jay-Lee Shir, and John A. Rogers[a)]
Department of Materials Science and Engineering, Department of Electrical and Computer Engineering, Department of Chemistry, Beckman Institute and Frederick Seitz Materials Research Laboratory, University of Illinois at Urbana-Champaign, Urbana, Illinois 61801

Alex Hamza
Lawrence Livermore National Laboratory, Livermore, California 94550

(Received 15 September 2006; accepted 8 November 2006; published online 18 December 2006)

Control of spectral bandwidth, illumination angle, and degree of collimation of light passing through a conformable phase mask provides an experimentally simple route to nanostructured materials with well defined depth gradients in density (i.e., porosity). In this approach, the illumination conditions define spatial variations in visibility of the distributions of intensity. Exposure of photopolymers to these intensity distributions generates, after developing, solid structures with geometries that compare well with expectation based on modeling of the optics. A range of structures is demonstrated, some of which have potential applications ranging from targets for laser fusion to vehicles for controlled release of chemicals. © *2006 American Institute of Physics*.
[DOI: 10.1063/1.2405386]

Wide ranging application possibilities in photonics, electronics, and biotechnology create intense interest in the formation of bulk materials that are structured, in well defined ways, on nanometer length scales.[1] There are two conceptual routes to such materials. The first uses bottom-up synthesis of building blocks (e.g., nanoparticles, nanowires, block copolymers, etc.) followed by guided or self-assembly into glassy, crystalline, or phase separated configurations. The second relies on top-down lithographic definition of nanostructured materials, in single or multiple step approaches, from bulk or thin film materials, using conventional or unconventional approaches. The deterministic control and the scalability to molecular dimensions represent main attractive features of these top-down and bottom-up routes, respectively. In the area of photonic crystals, as an example, the bottom-up methods include techniques such as colloidal sedimentation[2,3] and polymer phase separation.[4,5] Top-down approaches involve layer-by-layer photolithographic processes,[6] direct multiphoton writing,[7,8] multibeam holographic interferometric exposures,[9,10] and phase mask techniques.[11–13] Of these methods, the phase mask approaches are attractive because they are experimentally simple and scalable to large areas, they can define three dimensional (3D) nanostructured materials in a single step, and they can pattern systems that have aperiodic structures or localized defects. One variant, which we refer to as proximity field nanopatterning (PnP),[11,12] uses conformable, elastomeric phase masks that can achieve physical contact, and therefore optical alignment with nanometer precision in the out of plane direction, with photodefinable materials through the action of generalized adhesion forces.[14] This method also, unlike other related approaches, does not require conventional imaging systems, which can limit resolution and add cost and complexity; instead, all of the optics are built into the mask itself. In past work, this simple method was used to form a variety of 3D nanostructured materials, using exposure light from lasers and lamps with different wavelengths and polarizations, with masks having diverse geometries and photopolymers that show one as well as two photon sensitivities.[11,12,15,16]

In this letter, we show that control of spectral bandwidth, illumination angles, and degree of collimation in the exposure light enable additional important classes of 3D nanostructured materials to be formed with PnP. In particular, we present simple experimental routes to monotonic and nonmonotonic density graded nanoporous materials with applications that range from reservoir targets for shockless laser compression[17] to systems for controlled chemical or drug release.

Figure 1(a) schematically shows the experimental setup: the phase mask, the photosensitive layer, and the three exposure conditions that were explored. These conditions include the use of noncollimated light from a lamp (i), spectrally broad light from a lamp geometrically collimated with a hollow tube (ii), and multiple exposures, performed sequentially, at different illumination angles with the collimated output of a laser (iii). The lamp light (UVP Black Ray) consisted of the noncollimated output of 1.2 mW/cm^2 with 40 nm of full width at half maximum centered at ~350 nm. The laser light consisted of the frequency tripled output of a microchip neodymium-doped yttrium aluminum garnet laser (355 nm, Uniphase). Multiple exposures with this laser occurred at three angles (θ): normal to the surface (i.e., $\theta=0°$), $\theta=-\theta_0$, and $\theta=\theta_0$. We define the angular bandwidth as $\Delta\theta=2\theta_0$. The photosensitive material consisted of films (thickness ~10 μm) of a transparent epoxy (SU8, Microchem Corp.) spin coated on glass substrates and baked at 95 °C for 5 min. Surface embossed pieces of the elastomer poly(dimethylsiloxane) or perfluorinated poly(ether), fabricated according to procedures described elsewhere,[12] served as the phase masks. For experiments described here, we used masks with two different geometries. Mask 1 consisted of raised cylindrical posts with heights and diameters of 420 and 480 nm, respectively, with center to center separations of 600 nm and arranged in a hexagonal lattice. Mask 2 con-

[a)]Author to whom correspondence should be addressed; electronic mail: jrogers@uiuc.edu

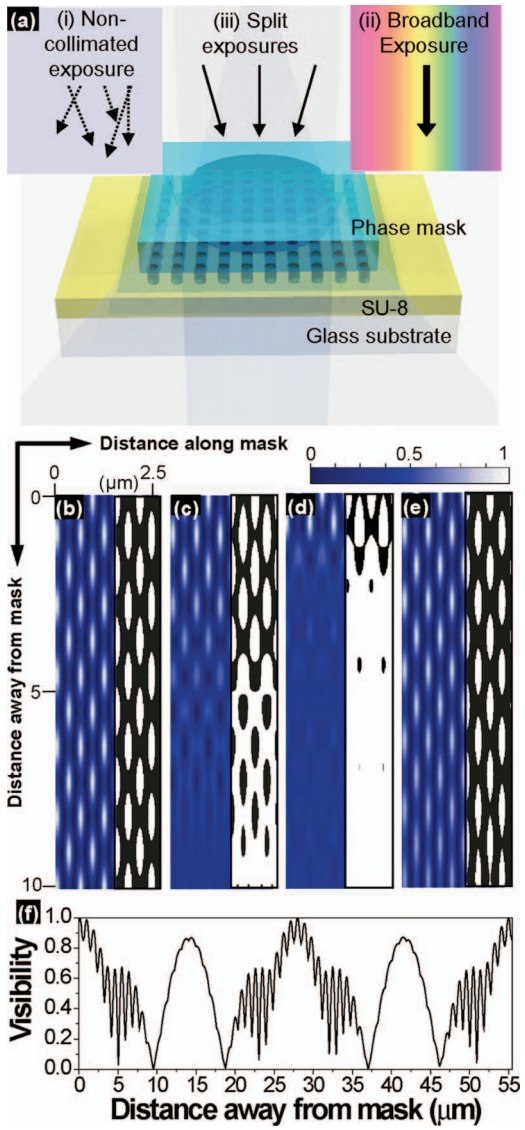

FIG. 1. (Color) (a) Schematic illustration showing various approaches to form density gradient structures. The middle frames show calculated intensity distributions and their binary cutoff images (strips located at the right side) for the case of phase grating ($n=1.4$; 300 nm raised lines spaced by 300 nm, with heights of 420 nm) in air ($n=1$) with the different exposure conditions illustrated in (a). The incident light consisted of TE polarized monochromatic (360 nm) plane waves. Intensity distributions (b) from $\Delta\theta=0°$, (c) from $\Delta\theta=2°$, (d) from $\Delta\theta=10°$, and (e) from superposition of wavelengths at 350, 355, 360, 365, 370, 375, and 380 nm. (f) Visibility as a function of distance away from the surface of the mask, for the case of $\Delta\theta=2°$.

sisted of posts with heights, diameters, and separations of 420, 375, and 566 nm, respectively, in a square lattice. Post-baking the exposed samples at 70 °C in an oven, developing away the unexposed regions, and supercritical drying completed the fabrication process.

Figures 1(b)–1(e) show rigorous coupled wave analysis results that illustrate the optics associated with each of the exposure conditions of Fig. 1. These calculations, for simplicity, used a grating-type phase mask with heights and linewidths of 420 and 300 nm (period $p=600$ nm) and a refractive index of 1.4. Passing monochromatic plane waves at $\lambda_0=360$ nm, linearly polarized along the direction of the mask lines (i.e., TE polarization), through the masks yielded the computed intensity distributions illustrated in Figs. 1(b)–1(e). The characteristic period of the variations in intensity (I) in the direction normal to the surface of the mask, known as the Talbot or self-imaging distance (d), is given by $\lambda_0/[1-(1-\lambda_0^2/p^2)^{0.5}]$.[18] The Talbot distance for this case is ~1800 nm, as shown in Fig. 1(b). These patterns of intensity create, through the exposure and development process outlined above, solid structures of the epoxy polymer. The visibility, as defined by $(I_{max}-I_{min})/(I_{max}+I_{min})$, determines, together with the exposure and development conditions, the amount of polymer that remains after development (i.e., the degree of porosity in the developed structures). This quantity, evaluated at a given distance from the surface of the mask, depends on the angular bandwidth of the exposure process, which is related, formally, to the spatial coherence length $\sim\lambda_0/\Delta\theta$, for the case of incoherent light.[19] Qualitatively, as the length decreases, the rate at which the visibility diminishes with distance from the surface of the mask increases. This behavior can be quantified by noting that the visibility, for the sequential laser exposures illustrated in Fig. 1, reaches a minimum when high and low intensity regions associated with different exposure angles overlap spatially. Exposures at small angles generate intensity distributions that are shifted by an amount equal to the product of the distance from the surface of the grating and the exposure angle. If we assume sequential, equal intensity exposures at $-\Delta\theta/2$, 0, and $\Delta\theta/2$, then the visibility reaches a minimum at a depth D, where the shifts of the intensity distributions associated with exposures at $-\Delta\theta/2$ and $\Delta\theta/2$ are equal to two-thirds of the grating period: $D=\frac{2}{3}p/\Delta\theta$. Writing this depth in terms of the number n of Talbot distances d by using the relation $d=2p^2/\lambda_0$ (for $\lambda_0 \gg p$) yields $n=\lambda_0/3p\Delta\theta$. This expression shows the direct proportionality of n on the spatial coherence. This derivation and the resulting expression are the same as that associated with commonly used definitions of the degree of coherence as determined by interference visibility.[19] By controlling, then, the angle between multiple exposures with a laser, it is possible to create a spatial depth gradient in the contrast ratio and, therefore, the degree of porosity in the developed structures. The frames of Figs. 1(c) and 1(d) that correspond to $\Delta\theta=2°$ and $\Delta\theta=10°$ show a substantial loss in visibility near the 11th and 2nd layers (one layer is equivalent to half Talbot distance), respectively, consistent with Eq. (3). Additionally, we note that for these types of laser exposures, the variation in visibility is periodic as a function of distance away from the surface of the mask, as shown in Fig. 1(f), thereby providing additional design flexibility.

Another parameter that can create such gradients is the spectral bandwidth of the exposure source, $\Delta\lambda$, as formally related to the temporal coherence length according to $\sim\lambda_0^2/\Delta\lambda$.[19] Qualitatively, the effect of spectral bandwidth is that different wavelength components generate intensity distributions with different characteristic Talbot distances (according to the equation above) in a way that reduces the visibility by an amount that depends on the bandwidth. As an approximation to effects associated with a continuous distribution of wavelengths, Fig. 1(e) shows computations that correspond to the linear addition of intensity patterns generated by light at 350, 355, 360, 365, 370, 375, and 380 nm. These wavelengths, which span the entire range of spectral sensitivity in the epoxy material used here, reduce the visibility only by a small amount for the distances and phase mask geometries considered here.

Figure 2 presents experimental results obtained in 3D nanostructures that demonstrate some of the effects. In all

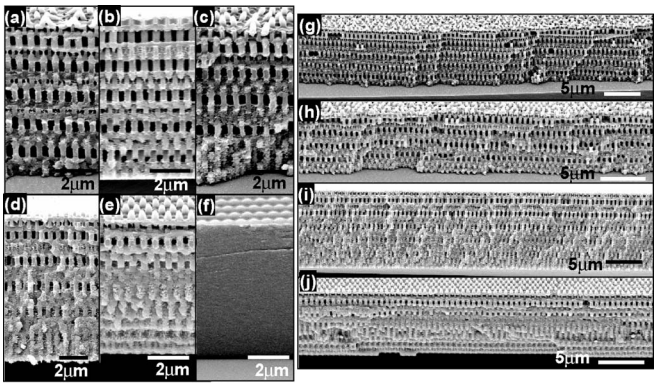

FIG. 2. Gradient nanostructured layers formed with optical exposures through a phase mask (mask 1), with various conditions. SEM images for multiple exposures with (a) $\Delta\theta=0°$, (b) $\Delta\theta=1°$, (c) $\Delta\theta=2°$, (d) $\Delta\theta=4°$, (e) $\Delta\theta=6°$, and (f) noncollimated exposure from a lamp. Large area views for (g) $\Delta\theta=0°$, (h) $\Delta\theta=2°$, (i) $\Delta\theta=4°$, and (j) $\Delta\theta=6°$.

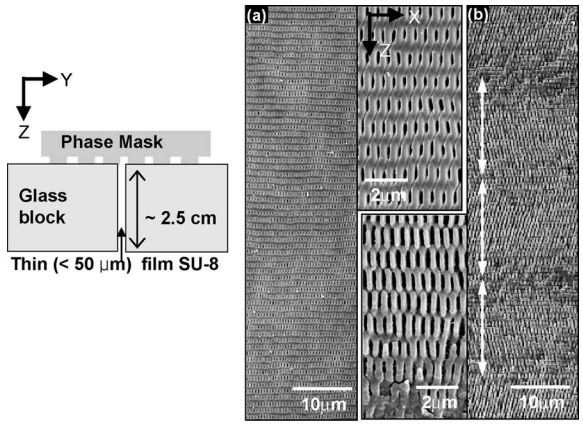

FIG. 3. Experimental setup (top frame) and SEM images of 3D structures formed with multiple exposures with (a) $\Delta\theta=0°$ and (b) $\Delta\theta=2°$ (incidents of 1, 0, −1°) with mask 2. The secondary periodicity (white arrows) in (b) is notable.

cases, exposures were performed through a conformable phase mask (mask 1) placed on the parts of the structures at the tops of these images. As the angular bandwidth of the sequential laser exposures increases from $\Delta\theta=0°$ [Figs. 2(a) and 2(g)] to 1° [Fig. 2(b)], 2° [Figs. 2(c) and 2(h)], 4° [Figs. 2(d) and 2(i)], and 6° [Figs. 2(e) and 2(j)], the spatial rate at which the porosity in the structures disappears with distance from their surfaces increases, consistent with expectation. In addition, the geometry of the structures at and near the top regions is insensitive to $\Delta\theta$, throughout this range; the phase mask determines the in-plane periodicity. For the mask geometries and exposure wavelengths explored here, we observed no significant effects of polarization. Exposures using the uncollimated output of an UV lamp show substantial structure only near the surface. By contrast, collimated output of the same type of lamp yields 3D structures similar to those of Figs. 2(a) and 2(g).[12] For these lamp exposures, the spectral bandwidth (as adjusted by use of transmission filters with different bandwidths) does not strongly affect the results for this range of thicknesses, which is also consistent with simulations.

To examine behaviors at larger distances from the surface of the mask, we used a thin film of epoxy formed between two polished glass blocks, with the phase mask placed on one edge of the film and with the exposure light directed perpendicular to the thickness direction of the film. Slight index mismatch between the BK7 glass (1.55 at 355 nm) and the SU8 (1.66 at 355 nm) generates some interface reflections (~0.164% for angles of incidence that correspond to the first order diffracted beam in this case) that can influence fine features in structures. The dominant spatial Fourier component and the overall geometries are not affected. This geometry avoids limitations associated with slight optical absorption in the epoxy. Figure 3 shows results from such experiments, performed with $\Delta\theta=0$ and 2° using mask 2. Two features are notable. First, the structures are well defined at distances up to several millimeters from the surface of the mask. This large working distance is derived from the combined use of coherent exposure light, relatively large beam diameters (6 mm), and mask (4×4 mm^2) sizes. Second, the case of $\Delta\theta=2°$ shows gradient structures that vary periodically with distance from the mask as expected. This periodicity is related to moiré-type effects associated with the angled superposition of periodic patterns. The measured periodicity in Fig. 3(b) is ~16 μm, which is close to the calculated value (~14 μm). The ability to achieve these unusual types of 3D geometries adds flexibility to the patterning approach. These same effects occur in the formation of structures in Fig. 2, but are not visible due to periods that are large compared to the film thicknesses.

In summary, this paper provides some simple experimental routes to complex graded density nanostructures that could be useful for a range of applications.

This work is supported by DOE-LLNL Grant No. B529271 and NSF Grant No. DMI 03-55532 and by Frederick Seitz Materials Research Laboratory by DOE Grant No. DEFG02-91-ER45439.

[1] Y. Xia, J. A. Rogers, K. E. Paul, and G. M. Whitesides, Chem. Rev. (Washington, D.C.) **99**, 1823 (1999).
[2] P. V. Braun and P. Wiltzius, Nature (London) **402**, 603 (1999).
[3] Y. A. Vlasov, X. Z. Bo, J. C. Sturm, and D. J. Norris, Nature (London) **414**, 289 (2001).
[4] Y. Fink, A. M. Urbas, M. G. Bawendi, J. D. Joannopoulos, and E. L. Thomas, J. Lightwave Technol. **17**, 1963 (1999).
[5] A. M. Urbas, M. Maldovan, P. DeRege, and E. L. Thomas, Adv. Mater. (Weinheim, Ger.) **14**, 1850 (2002).
[6] S. Y. Lin, J. G. Fleming, D. L. Hetherington, B. K. Smith, R. Biswas, K. M. Ho, M. M. Sigalas, W. Zubrzycki, S. R. Kurtz, and J. Bur, Nature (London) **394**, 251 (1998).
[7] H.-B. Sun and S. Kawata, Adv. Polym. Sci. **170**, 169 (2004).
[8] M. Deubel, G. Von Freymann, M. Wegener, S. Pereira, K. Busch, and C. M. Soukoulis, Nat. Mater. **3**, 444 (2004).
[9] M. Campbell, D. N. Sharp, M. T. Harrison, R. G. Denning, and A. J. Turberfield, Nature (London) **404**, 53 (2000).
[10] C. K. Ullal, M. Maldovan, E. L. Thomas, G. Chen, Y.-J. Han, and S. Yang, Appl. Phys. Lett. **84**, 5434 (2004).
[11] S. Jeon, V. Malyarchuk, J. A. Rogers, and G. P. Wiederrecht, Opt. Express **14**, 2300 (2006).
[12] S. Jeon, J.-U. Park, R. Cirelli, S. Yang, C. E. Heitzman, P. V. Braun, P. J. A. Kenis, and J. A. Rogers, Proc. Natl. Acad. Sci. U.S.A. **101**, 12428 (2004).
[13] T. Y. M. Chan, O. Toader, and S. John, Phys. Rev. E **73**, 046610 (2006).
[14] Y. G. Y. Huang, W. X. Zhou, K. J. Hsia, E. Menard, J. U. Park, J. A. Rogers, and A. G. Alleyne, Langmuir **21**, 8058 (2005).
[15] S. Jeon, E. Menard, J.-U. Park, J. Maria, M. Meitl, J. Zaumseil, and J. A. Rogers, Adv. Mater. (Weinheim, Ger.) **16**, 1369 (2004).
[16] S. Jeon, V. Malyarchuk, J. O. White, and J. A. Rogers, Nano Lett. **5**, 1351 (2005).
[17] R. F. Smith, K. T. Lorenz, D. Ho, B. A. Remington, A. Hamza, J. A. Rogers, S. Jeon, Y.-S. Nam, and J. Kilkenny (unpublished).
[18] E. Noponen and J. Turunen, Opt. Commun. **98**, 132 (1993).
[19] M. V. Klein, *Optics* (Wiley, New York, 1970), p. 272.